nature medicine

LETTERS

https://doi.org/10.1038/s41591-018-0106-7

Fetal gene therapy for neurodegenerative disease of infants

Giulia Massaro[1], Citra N. Z. Mattar[2], Andrew M. S. Wong[3], Ernestas Sirka[4], Suzanne M. K. Buckley[5], Bronwen R. Herbert[6], Stefan Karlsson[7], Dany P. Perocheau[5], Derek Burke[8], Simon Heales[8], Angela Richard-Londt[9], Sebastian Brandner[9], Mylene Huebecker[10], David A. Priestman[10], Frances M. Platt[10], Kevin Mills[4], Arijit Biswas[2], Jonathan D. Cooper[3,11,12], Jerry K. Y. Chan[2,13,14], Seng H. Cheng[15], Simon N. Waddington[5,16*] and Ahad A. Rahim[1]

For inherited genetic diseases, fetal gene therapy offers the potential of prophylaxis against early, irreversible and lethal pathological change. To explore this, we studied neuronopathic Gaucher disease (nGD), caused by mutations in *GBA*. In adult patients, the milder form presents with hepatomegaly, splenomegaly and occasional lung and bone disease; this is managed, symptomatically, by enzyme replacement therapy. The acute childhood lethal form of nGD is untreatable since enzyme cannot cross the blood–brain barrier. Patients with nGD exhibit signs consistent with hindbrain neurodegeneration, including neck hyperextension, strabismus and, often, fatal apnea[1]. We selected a mouse model of nGD carrying a *loxP*-flanked neomycin disruption of *Gba* plus Cre recombinase regulated by the keratinocyte-specific K14 promoter. Exclusive skin expression of *Gba* prevents fatal neonatal dehydration. Instead, mice develop fatal neurodegeneration within 15 days[2]. Using this model, fetal intracranial injection of adeno-associated virus (AAV) vector reconstituted neuronal glucocerebrosidase expression. Mice lived for up to at least 18 weeks, were fertile and fully mobile. Neurodegeneration was abolished and neuroinflammation ameliorated. Neonatal intervention also rescued mice but less effectively. As the next step to clinical translation, we also demonstrated the feasibility of ultrasound-guided global AAV gene transfer to fetal macaque brains.

Antibodies against activated microglia (CD68) and astrocytes (glial fibrillary acid protein, GFAP) were used to assess spatiotemporal neuroinflammation and gliosis in the nGD mouse and this was quantified by thresholding image analysis. Unlike wild types (WTs) and heterozygotes, brains of symptomatic post-gestational day (P)12 knockouts exhibited significant and widespread microglial activation (Supplementary Fig. 1c) particularly in the Gi of the brainstem, the VPM/VPL and layer V of the S1BF. Blinded semi-quantitative scoring revealed that no region was spared (Supplementary Table 1). This was confirmed by immunostaining for a second microglial marker, Iba1 (Supplementary Fig. 1f). Significant astrogliosis (Supplementary Fig. 2c) was confirmed by both thresholding analysis and blinded scoring (Supplementary Table 2). At presymptomatic age P8, knockout mouse brains showed significant microglial (Supplementary Fig. 1b) and astrocyte (Supplementary Fig. 2b) activation in the thalamus and brainstem. Blinded scoring (Supplementary Tables 1 and 2) and Iba1 immunohistochemistry (Supplementary Fig. 1e) provided confirmation. Remarkably, even in P1 neonates there was significant activation of astrocytes (Fig. 1a–c) and microglia (Fig. 1d–f) in the brainstem.

Neuronal loss was quantified by stereological assessment of Nissl-stained coronal sections. There was significant neuronal loss in the cortex, thalamus and brainstem of knockouts at P12 (Supplementary Fig. 3b), accompanied by acellular spaces consistent with either large vacuole formation or lipid accumulation as determined by hematoxylin and eosin staining (Supplementary Fig. 3c). In P8 knockouts, there was significant loss of cortical and midbrain neurons (Supplementary Fig. 3a). Neuronal loss correlated with microglial and astrocyte activation and, consistent with findings in a milder nGD model[3], there was significant cortical thinning in S1BF (Supplementary Fig. 3d); however, no difference in volume was observed (Supplementary Fig. 3e).

In the absence of functional glucocerebrosidase (GCase), its substrate, glucosylceramide (D-glucosyl-β1-1′-*N*-acyl-D-*erythro*-sphingosine), and related sphingolipid species accumulate in both humans and mouse models[4]. Total glucosylceramide and glucosylsphingosine are elevated >20-fold at birth in the nGD mouse[5], but no detailed measurements of different glucosylceramide species and proximal metabolites have been made. We assembled a temporal profile in whole-brain homogenates using liquid chromatography and tandem mass spectrometry. In knockouts, all glucosylceramide species except for C24:0-OH and C24:1-OH were significantly elevated at P1, C18:0 and C16:0 being most abundant (Fig. 1g and

[1]UCL School of Pharmacy, University College London, London, UK. [2]Department of Obstetrics and Gynaecology, Yong Loo Lin School of Medicine, National University of Singapore, Singapore, Singapore. [3]Department of Basic and Clinical Neuroscience, King's College London, Institute of Psychiatry, Psychology and Neuroscience, London, UK. [4]UCL Great Ormond Street Institute of Child Health, University College London, London, UK. [5]UCL Institute for Women's Health, University College London, London, UK. [6]Institute for Reproductive and Developmental Biology, Imperial College London, London, UK. [7]Division of Molecular Medicine and Gene Therapy, Lund University, Lund, Sweden. [8]Paediatric Laboratory Medicine, Great Ormond Street Hospital and UCL Great Ormond Street Institute of Child Health, London, UK. [9]Department of Neurodegenerative Disease, UCL Institute of Neurology, University College London, London, UK. [10]Department of Pharmacology, University of Oxford, Oxford, UK. [11]Department of Pediatrics, Los Angeles Biomedical Research Institute at Harbor–UCLA Medical Center, David Geffen School of Medicine, University of California Los Angeles, Torrance, CA, USA. [12]Department of Pediatrics, Washington University School of Medicine, St Louis, MO, USA. [13]Department of Reproductive Medicine, KK Women's and Children's Hospital, Singapore, Singapore. [14]Cancer and Stem Cell Biology, Duke-NUS Medical School, Singapore, Singapore. [15]Sanofi, Framingham, MA, USA. [16]MRC Antiviral Gene Therapy Research Unit, Faculty of Health Sciences, University of the Witswatersrand, Johannesburg, South Africa. *e-mail: s.waddington@ucl.ac.uk

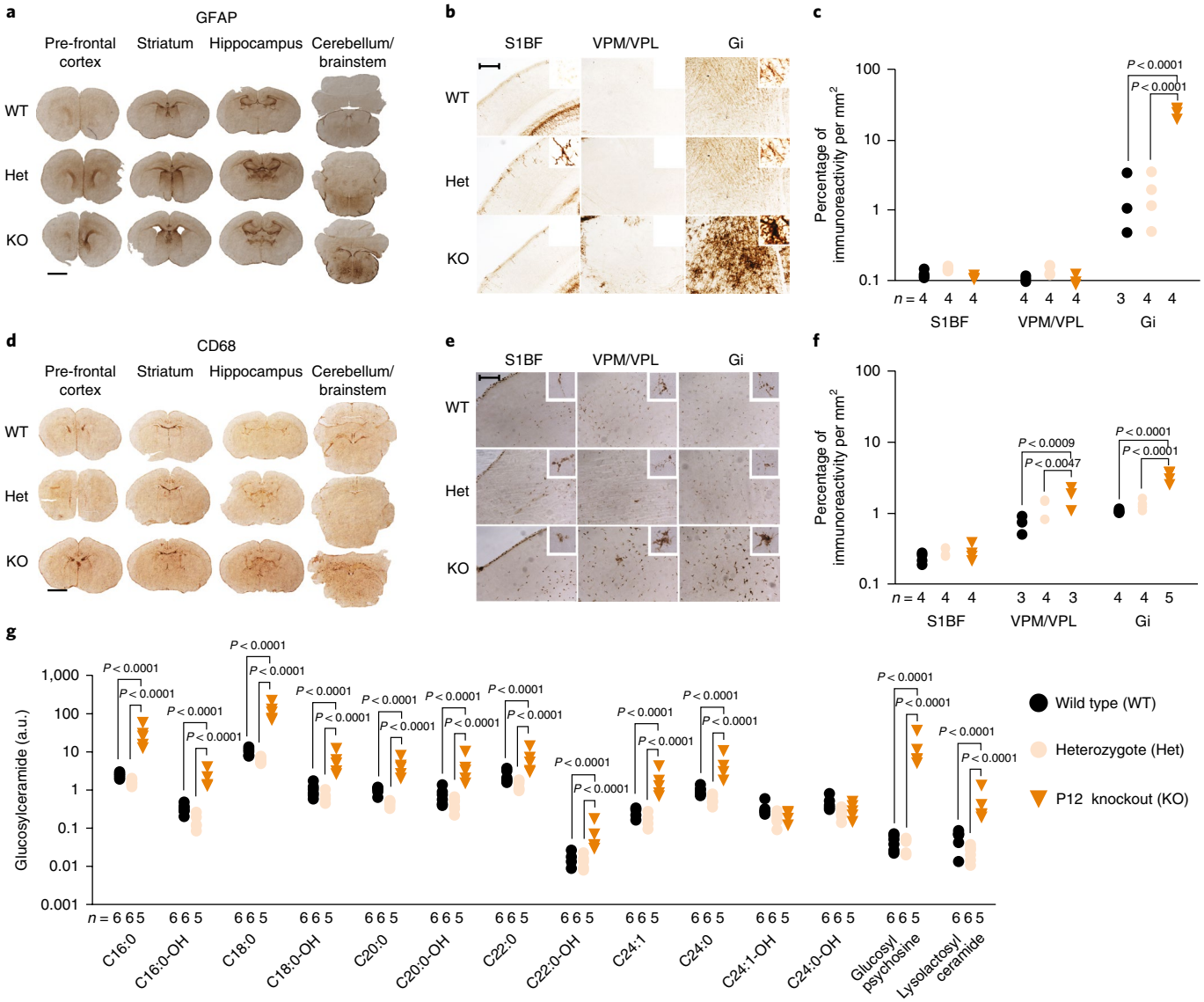

Fig. 1 | Brain disease at birth in nGD mice. a, GFAP immunostaining in newborn knockout, heterozygous and WT brains. Scale bar, 1 mm. **b**, Higher magnification of **a** in the somatosensory barrel field cortex (S1BF), ventral posteromedial/posterolateral nuclei (VPM/VPL) and gigantocellular nucleus (Gi). Scale bar, 0.25 mm. **c**, Quantification of **b** (two-way analysis of variance (ANOVA), Tukey's multiple comparison). **d**, CD68 immunohistochemistry in newborn knockout, heterozygous and WT brains. Scale bar, 1 mm. **e**, Higher magnification of **d**. Scale bar, 0.25 mm **f**, Quantification of **e** (two-way ANOVA). **g**, Mass spectrometry analysis of glucosylceramide isoforms, glucopsychosine and lyso-lactosylceramide in knockout, heterozygote and WT brains (two-way ANOVA on log-transformed data; Bonferroni's multiple comparison). Numbers of mice are stated under each group.

Supplementary Fig. 4a); glucosylpsychosine was increased the most (Supplementary Table 3). At P8 and P12, these remained the most elevated in both absolute (Supplementary Fig. 4b,c) and relative (Supplementary Table 3) terms. As expected, the gangliosides GM1a, GD1a, GD1b and GTb remained unchanged in knockouts irrespective of their age (Supplementary Fig. 4d–f).

The upregulation of neuroinflammatory markers and glycosphingolipids in P1 knockouts suggested that prophylactic in utero gene therapy might be beneficial. We selected adeno-associated virus serotype 9 (AAV9) as we[6], and others[7], have observed widespread neuronal expression of green fluorescent protein (GFP), following fetal intracranial injection. We examined the expression profile after fetal intracranial injection of an AAV9 vector encoding GFP driven by a β-glucuronidase (GUSB) promoter[8] (Supplementary Fig. 5a). At 16 days of gestation, fetuses received 5 µl of AAV9 vector (5×10^{10} genome copies) into the lateral ventricle. At 30 days of age, strong bilateral fluorescence extended from the olfactory bulbs to the brainstem (Supplementary Fig. 5b). Bilateral homogeneity of expression and extensive spread from prefrontal cortex to cerebellum and brainstem was confirmed by immunohistochemistry (Supplementary Fig. 5c). Many GFP-expressing cells with neuronal morphology were observed in the cortex, striatum, hippocampus, thalamus, cerebellum and, importantly, brainstem (Supplementary Fig. 5d).

Using the same vector configuration, mode and timing of injection, we delivered human AAV9-GBA[9] into pups of *Gba* heterozygous parents. While impossible to genotype in utero, we identified three knockouts after birth by assay of GCase activity in blood spots obtained by superficial temporal vein puncture. They exhibited neither paralysis nor dyskinesia, remaining indistinguishable from WT littermates until being euthanized at 35 days of age. Treated knockouts had substantially diminished microglial and

astrocyte activation versus untreated P12 knockouts in the prefrontal cortex, striatum, hippocampus and cerebellum (Fig. 2a,b and Supplementary Fig. 6a,b) and there was a tendency for greater treatment effects in Gi than S1BF (Supplementary Fig. 6d,e).

Lysosomal-associated membrane protein 1 (LAMP-1) is increased in fibroblasts of a patient with nGD[10], and was, therefore, selected as a more direct marker of lysosomal compartment size. P12 knockout brains showed strong LAMP-1 expression compared with P35 WT mice. In contrast, staining was similar in treated knockouts and WT mice, with the exception of a few, sparse darkly stained LAMP-1-positive cells in treated knockouts (Fig. 2c and Supplementary Fig. 6c).

Gene therapy prevented neuronal loss in knockouts in the thalamus and Gi (Fig. 2d). Staining with two anti-GCase antibodies indicated that normal enzyme expression had been restored, yet each provided different insights. A carboxy-terminus-specific antibody showed that WT and AAV9-treated knockouts exhibited discrete GCase immunoreactivity within neurons, which was completely absent in untreated knockouts. In contrast, an amino-terminal antibody revealed strong staining of glia rather than neurons in all cortical layers, which was absent in WT brains. After AAV9 treatment of knockouts, staining was observed in neurons in the deeper cortical layers but not in glia (Fig. 2e).

To test long-term efficacy, we injected five knockouts (two males and three females, three separate litters). Consistent with the description of the model[2], 7 untreated control knockouts developed forelimb paralysis and then tetraparesis; 5 and 2 mice were euthanized at humane endpoints at 14 and 15 days of age. In contrast, at 70 days of age, all treated knockouts appeared normal and fertile, and 2 were able to produce a litter of 2 symptomatic knockouts (Supplementary Video 1). One treated mouse was euthanized at 125 days after exhibiting stereotypic circling behavior and another at 131 days because of an untreatable eye infection; at which time the remainder were then euthanized (Fig. 2f). GCase activity in brain homogenates of treated mice was not significantly different from WTs (Fig. 2g). Paradoxically, other parameters indicated only partial correction of the disease phenotype. Treated knockouts tended to perform worse on Rotarod (Fig. 2h) and grid walk (Fig. 2i) tests. At 100 days, they weighed significantly less than unaffected littermates (Fig. 2j) and appeared hyperkinetic (Supplementary Video 2). They exhibited significant elevation of the shorter chain glycosphingolipids, glucosylpsychosine and lyso-lactosyl ceramide (Fig. 2k) and GD1a (Supplementary Fig. 6g) but not glucosylceramide (Supplementary Fig. 6h). Microglial activation (Supplementary Fig. 6i) and astrogliosis (Supplementary Fig. 6j) was ameliorated but not normalized and four of the five mice exhibited ventriculomegaly.

To test the efficacy of gene therapy later in development, newborn (P0–P1) knockouts received intracerebroventricular injection of 5 µl AAV9 vector (5.0×10^{10} genome copies). Previous studies have demonstrated the ability of intravenous AAV9 to cross the blood–brain barrier of neonatal mice[11,12] and non-human primates[11] resulting in efficient expression in neural cells and viscera[13]. Therefore, we also tested whether an intravenous administration of the AAV9 vector (4×10^{11} genome copies) to knockouts could ameliorate both visceral and brain pathology. Both treated cohorts were rescued from neonatal death, exhibited neither paralysis nor dyskinesia and remained indistinguishable from WTs until being euthanized at 55 days of age (Fig. 3a). There were no significant differences in weight (Fig. 3b) or motor coordination (Fig. 3c) between treated knockouts and WTs.

There was significant supraphysiological expression of GCase in the cortical S1BF region, CENT2 of the cerebelleum and Gi, and physiological levels in the hippocampal CA1–CA2 and thalamic VPM/VPL regions (Fig. 3d). There was no significant increase in astrogliosis in the CA1–CA2, VPM/VPL and Gi regions of intravenously injected knockouts at 55 days (Fig. 3e); however, there was a significant increase in the S1BF, VPM/VPL and CENT2 regions. There was no significant increase in microglial activation between the treated mice in any region except S1BF (Fig. 3f). Furthermore, the untreated 14-day-old knockout nGD mice showed a significantly higher amount of staining compared to the older intravenously treated mice in the VPM/VPL and Gi regions. There was no significant increase in the lysosomal marker LAMP-1 in any region except Gi (Fig. 3g). There was no significant loss of neurons in the Gi of knockout mice treated with intravenous gene therapy (Fig. 3h). However, there was a significant loss in the cortical S1BF and thalamic VPM/VPL regions. The cortex was significantly thinner in intravenously injected knockouts (Fig. 3h). Despite overall strong GCase staining in the S1BF region and the cerebral cortex neuroinflammation, neuronal loss and subsequent cortical thinning were still evident.

After both intracerebroventricular and intravenous injection, GCase was significantly elevated in visceral organs (Fig. 3i), suggesting vector escape from the brain after intracerebroventricular administration. Intravenous gene therapy normalized enzyme activity in all visceral organs except the heart, where activity was supraphysiological. Intravenous gene therapy prevented splenomegaly (Fig. 3j) and Gaucher cell infiltration in spleen, liver and lungs. In contrast, intracerebroventricular injection failed to prevent Gaucher cell infiltration in spleen (Fig. 3k), liver (Fig. 3l) and lungs (Fig. 3m), as confirmed by immunohistochemistry. Therefore, while intracerebroventricular gene therapy is effective in treating the lethal neuropathology, it does not ameliorate the visceral manifestations. However, intravenous administration effectively limits both neurological and visceral pathology.

Separate groups were assessed for long-term efficacy. All treated mice survived to at least 180 days and were indistinguishable from age-matched WTs (Fig. 3n). Spleens from intracerebroventricular injection cohorts were significantly heavier than those receiving intravenous injection (Fig. 3p). Large Gaucher cells were present in the spleens following intracerebroventricular, but not intravenous injection (Fig. 3o).

We next asked whether in utero gene delivery could achieve widespread expression in the larger, gyrencephalic primate brain by performing ultrasound-guided delivery of AAV9 vectors to mid-gestation fetal macaques. Cerebrospinal fluid flows from the lateral ventricles through the ventricular system to the central canal of the spinal cord and the subarachnoid cisterns. Therefore, to achieve maximum vector spread, we identified the lateral cerebral ventricles of two day-58 (0.4G) macaque fetuses by transabdominal ultrasound. Vector was injected into the right lateral ventricle under ultrasound guidance. scAAV9-GUSB-GFP was administered at a concentration of 6.6×10^{12} vector genomes (vg) ml^{-1} over 60 s. Correct delivery was confirmed by observation of transient (10 min) ventricular swelling (Fig. 4a). Both macaques presented normally at birth. There was extensive and bilateral rostro-caudal expression of GFP (Fig. 4b) with numerous GFP-positive cells of neuronal morphology in the superior frontal and middle temporal gyri, thalamus, hippocampus, uvula and Gi (Fig. 4c). Most other brain regions contained immunopositive cells except for, particularly, the caudate nucleus and putamen (Supplementary Fig. 7). No discrete cells were observed in unstained brain (Figs. 4b,c and Supplementary Fig. 7).

The sustained, widespread gene expression from a single vector injection is supported by a recent study in non-human primate studies and clinical trials. At least 15 years of AAV-mediated transgene expression has been demonstrated in a non-human primate model of Parkinson's disease[14]. Proof-of-concept has already been provided for single-dose sustained long-term AAV expression in liver-directed gene therapy for the treatment of hemophiliac patients[15].

Widespread gene delivery to the central nervous system by fetal intracranial injection offers the best therapeutic potential for inherited early onset neurodegenerative diseases affecting the whole

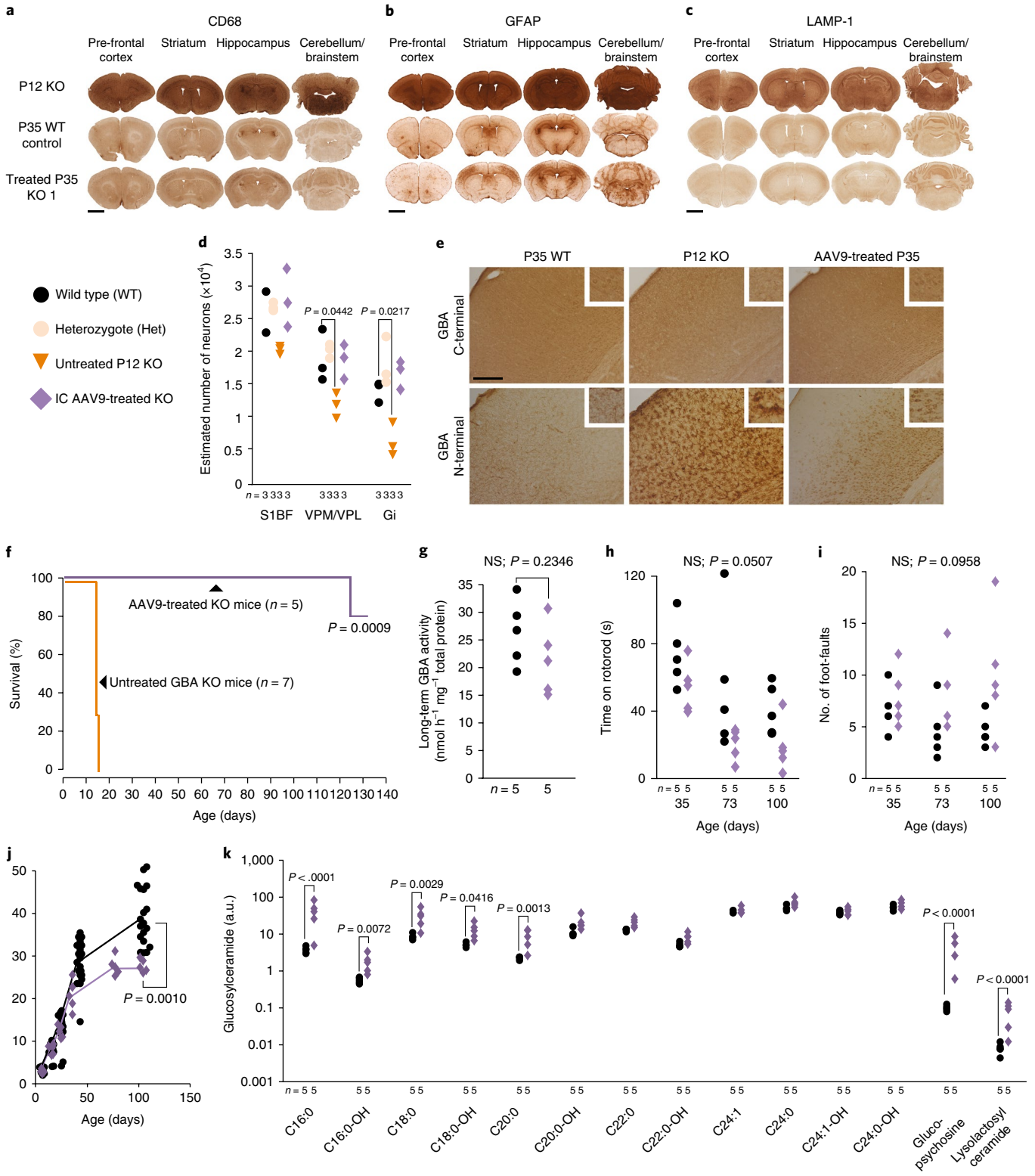

Fig. 2 | Fetal gene therapy of nGD mice. a–**c**, CD68 (**a**), GFAP (**b**) and LAMP-1 (**c**) brain immunostaining of untreated P12 knockouts and P35 WT and treated mice from different litters (scale bars, 1 mm). **d**, Stereological estimates of neuron number in the brains of treated knockout, heterozygote, WT and untreated day-12 knockouts (two-way ANOVA, Bonferroni's multiple comparison, all versus WT). (Representative of 3 KO replicates shown in Supplementary Fig. 6.) **e**, GCase C-terminal antibody labeling neurons in WT, knockout and treated knockout brains. N-terminal antibody staining in WT and treated knockouts (S1BF images, scale bar, 0.25 mm). Representative of three mice replicates per experimental cohort. **f**, Survival studies of treated knockouts compared to untreated knockouts (Mantel–Cox test, $n=5$ and 7 mice, respectively). **g**, GCase enzyme activity in treated and WT brains (Student's one-tailed t-test). **h**,**i**, Rotarod (**h**) and foot-fault (**i**) tests on treated knockout and WT mice (two-way ANOVA, Bonferroni's multiple comparison). **j**, Weights of treated and WT mice over time (Student's one-tailed t-test on weight at 100 days, WT $n=19$, KO $n=5$). **k**, Mass spectrometry profiles in the brains of treated knockout and WT mice (two-way ANOVA on log-transformed data, Bonferroni's multiple comparison). Numbers of mice are stated under each group. NS, not significant.

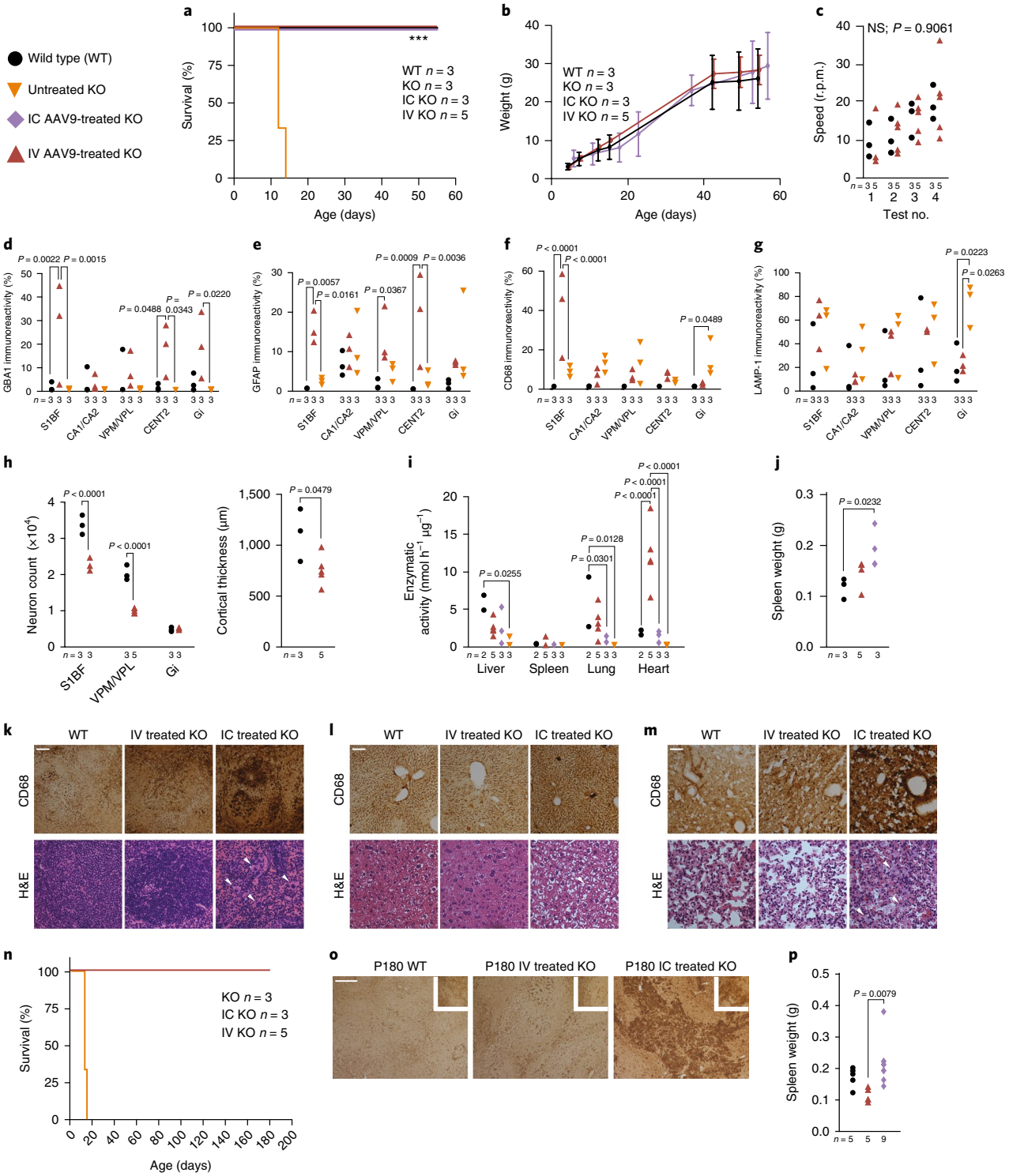

Fig. 3 | Intracerebroventricular and intravenous gene therapy in neonatal nGD mice. a, Kaplan–Meier survival plot of untreated knockouts, intracerebroventricular (IC) gene-therapy-treated knockouts, intravenous (IV) gene-therapy-treated knockouts and WTs (log-rank, Mantel–Cox test). **b**, Weights of mice from **a** (mean ± s.d.). **c**, Rotarod assessment of mice from **a** (repeated-measures ANOVA). **d**–**g**, Immunohistochemistry for GBA (**d**), GFAP (**e**), CD68 (**f**) and LAMP-1 (**g**) in brains of 55-day-old treated knockouts and WTs and P12 untreated knockouts in the S1BF, hippocampal cornu ammonus 1 (CA1), the cerebellar central lobule II (CENT2) and Gi (two-way ANOVA, Tukey's multiple comparisons). **h**, Neuron counts in the Gi, S1BF and VPM/VPL in treated knockouts and WTs and cortical thickness measurements (two-way ANOVA, Tukey's multiple comparisons). **i**, GCase activity in organs of treated knockouts, WTs and untreated P12 knockouts (two-way ANOVA, Tukey's multiple comparisons). **j**, Spleen weights from mice receiving gene therapy and WTs (one-way ANOVA, Tukey's multiple comparisons). **k**–**m**, Hemotoxylin and eosin staining and CD68 immunohistochemistry of spleens (**k**), livers (**l**) and lungs (**m**) from intravenously and intracerebroventricularly gene-therapy-treated and WT mice (white arrows highlight Gaucher cells; scale bars, 0.1 mm). **n**, Kaplan–Meier survival plot of long-term gene-therapy-treated and untreated knockouts (Mantel–Cox test). **o**, CD68 immunohistochemistry on spleens from **n** and WTs (scale bar, 0.25 mm). **p**, Spleen weights from **o** (one-way ANOVA, Tukey's multiple comparisons). Numbers of mice are stated under each group. NS, not significant.

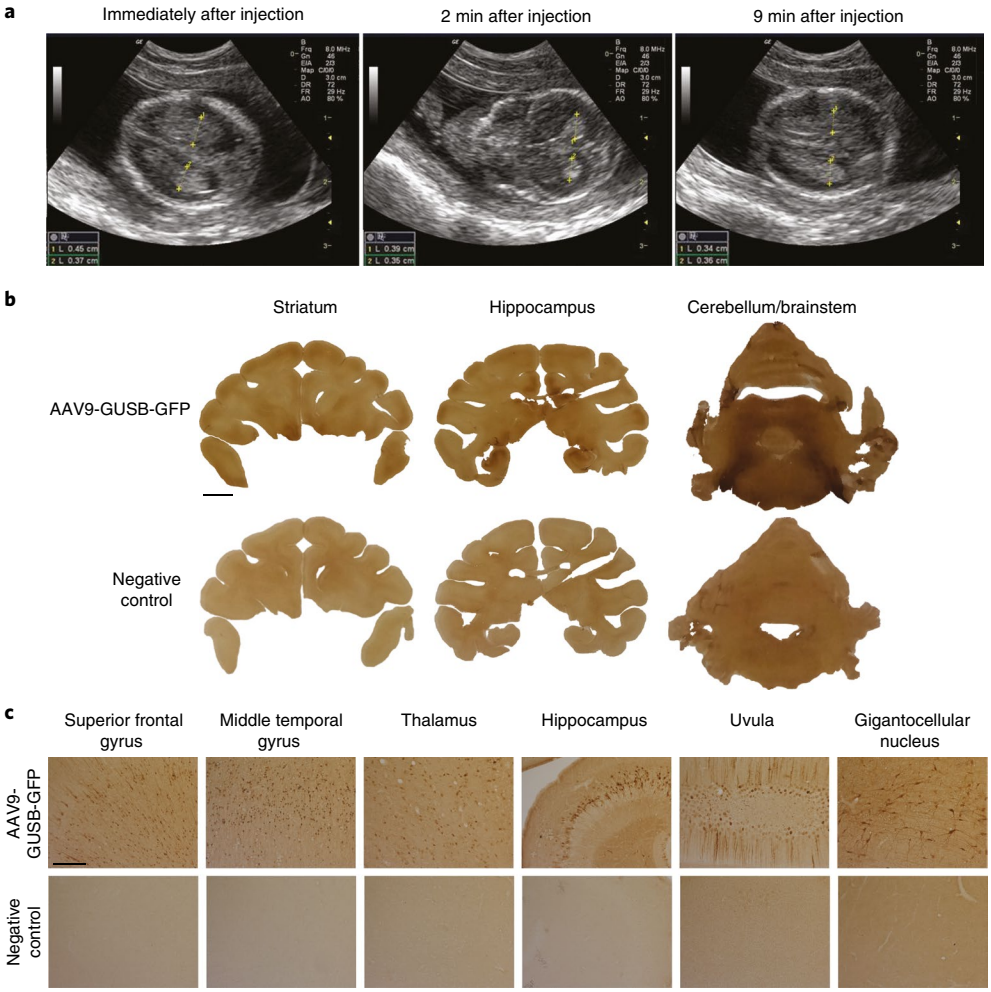

Fig. 4 | In utero gene delivery to the macaque brain via ultrasound-guided intracerebroventricular injection of vector. a, Ultrasound images following intracerebroventricular administration over time. **b**, Green fluorescent protein immunohistochemistry on brain sections from administered macaques and control. Scale bar, 5 mm. **c**, Higher-magnification examination of **b**. Scale bar, 0.25 mm. Representative of two administered macaque replicates.

brain. Delivery to the developing central nervous system may be especially important since neurons have limited regenerative capacity. This is evidenced by the fact that neonatal vector delivery was less effective than fetal intervention in averting neuronal loss. Of several studies on in utero gene therapy in gene-disrupted mice[16], none involved models where pathology is already evident at birth and fetal intervention is the only tractable approach. Recent gene therapy clinical trials for mucopolysaccharidosis type IIIa and spinal muscular atrophy[17] indicate that the youngest patients derived most therapeutic benefit[18].

Normalization of GCase activity in the brain did not completely abolish pathology. Knockouts receiving intracerebroventricular injection developed visceral disease. Hypermetabolism, previously identified in patients with Gaucher[19], may account for their lower body mass. However, this would not explain the failure to normalize brain glycosphingolipids, nor prevent long-term microglial and astrocyte activation and ventriculomegaly. AAV gene delivery follows a Poisson distribution[20]. Therefore, individual neurons may receive variable gene dosage, with some remaining un-transduced, as evidenced by heterogeneous staining in treated knockout brains (Fig. 2e).

Human fetal gene therapy necessitates accurate prenatal diagnosis. From cell-free fetal DNA in the maternal circulation, founder mutations underlying Gaucher disease can be detected non-invasively[21]. Concerns over weak genotype–phenotype correlation can be mitigated: several lysosomal storage diseases, including Gaucher disease, have been diagnosed by enzyme assay of chorionic villi samples[22]. Currently, prenatal screening is usually restricted to a family with a history of Gaucher disease or parents of an affected child, although advances in non-invasive prenatal diagnosis may help identify most cases.

Perinatal gene transfer has been shown to reduce or avoid an immune response to either a protein (absent in an animal model and potentially also in some patients), or to a viral capsid protein[23,24]. Immune tolerance may permit vector re-administration. The presence of GCase in the skin of the knockout nGD mice precluded us from investigating this specifically. Nevertheless, immune tolerance towards a non-mammalian protein following fetal or neonatal gene delivery has been observed in non-human primate studies[25] and in mice this allowed effective re-administration of vector[26]. Avoidance of an immune response following gene therapy is important. Non-human primates seropositive for AAV9 are less efficiently transduced using an AAV9 vector[27]. Prednisolone was used in a recent AAV9 gene therapy clinical trial for spinal muscular atrophy to manage anti-vector immune responses[17]. While this effectively managed the immune response, in utero administration of vector may pre-empt exposure to WT AAV and thus development of anti-capsid immunity.

This study highlights the potential of fetal gene therapy for neonatal lethal neurodegenerative diseases; the non-human

primate data offer a clinically feasible protocol for its implementation. This, and other preclinical fetal gene therapy studies, address the suggested requirements of the NIH recombinant DNA advisory committee[28], namely safety and efficacy in relevant models for progression to clinical trials.

Methods

Methods, including statements of data availability and any associated accession codes and references, are available at https://doi.org/10.1038/s41591-018-0106-7.

Received: 20 June 2016; Accepted: 25 May 2018;
Published online: 16 July 2018

References

1. Gupta, N., Oppenheim, I. M., Kauvar, E. F., Tayebi, N. & Sidransky, E. Type 2 Gaucher disease: phenotypic variation and genotypic heterogeneity. *Blood Cells Mol. Dis.* **46**, 75–84 (2011).
2. Enquist, I. B. et al. Murine models of acute neuronopathic Gaucher disease. *Proc. Natl Acad. Sci. USA* **104**, 17483–17488 (2007).
3. Farfel-Becker, T. et al. Spatial and temporal correlation between neuron loss and neuroinflammation in a mouse model of neuronopathic Gaucher disease. *Hum. Mol. Genet.* (2011).
4. Farfel-Becker, T. et al. Neuronal accumulation of glucosylceramide in a mouse model of neuronopathic Gaucher disease leads to neurodegeneration. *Hum. Mol. Genet.* (2013).
5. Cabrera-Salazar, M. A. et al. Systemic delivery of a glucosylceramide synthase inhibitor reduces CNS substrates and increases lifespan in a mouse model of type 2 Gaucher disease. *PLoS ONE* **7**, e43310 (2012).
6. Rahim, A. A. et al. In utero administration of Ad5 and AAV pseudotypes to the fetal brain leads to efficient, widespread and long-term gene expression. *Gene Ther.* **19**, 936–946 (2012).
7. Haddad, M. R., Donsante, A., Zerfas, P. & Kaler, S. G. Fetal brain-directed AAV gene therapy results in rapid, robust, and persistent transduction of mouse choroid plexus epithelia. *Mol. Ther. Nucleic Acids* **2**, e101 (2013).
8. Passini, M. A. & Wolfe, J. H. Widespread gene delivery and structure-specific patterns of expression in the brain after intraventricular injections of neonatal mice with an adeno-associated virus vector. *J. Virol.* **75**, 12382–12392 (2001).
9. Sardi, S. P. et al. CNS expression of glucocerebrosidase corrects α-synuclein pathology and memory in a mouse model of Gaucher-related synucleinopathy. *Proc. Natl Acad. Sci. USA* (2011).
10. Zimmer, K. P. et al. Intracellular transport of acid β-glucosidase and lysosome-associated membrane proteins is affected in Gaucher's disease (G202R mutation). *J. Pathol.* **188**, 407–414 (1999).
11. Foust, K. D. et al. Intravascular AAV9 preferentially targets neonatal neurons and adult astrocytes. *Nat. Biotechnol.* **27**, 59–65 (2009).
12. Rahim, A. A. et al. Intravenous administration of AAV2/9 to the fetal and neonatal mouse leads to differential targeting of CNS cell types and extensive transduction of the nervous system. *FASEB J.* **25**, 3505–3518 (2011).
13. Mattar, C. N. et al. Systemic delivery of scAAV9 in fetal macaques facilitates neuronal transduction of the central and peripheral nervous systems. *Gene Ther.* **20**, 69–83 (2013).
14. Sehara, Y. et al. Persistent expression of dopamine-synthesizing enzymes 15 years after gene transfer in a primate model of Parkinson's disease. *Hum. Gene Ther. Clin. Dev.* **28**, 74–79 (2017).
15. Nathwani, A. C. et al. Long-term safety and efficacy of factor IX gene therapy in hemophilia B. *N. Engl. J. Med.* **371**, 1994–2004 (2014).
16. McCain, L. & Flake, A. W. In utero stem cell transplantation and gene therapy—recent progress and the potential for clinical application. *Best Pract. Res Clin Obstet. Gynaecol.* (2015).
17. Mendell, J. R. et al. Single-dose gene-replacement therapy for spinal muscular atrophy. *N. Engl. J. Med.* **377**, 1713–1722 (2017).
18. Tardieu, M. et al. Intracerebral administration of AAV rh.10 carrying human SGSH and SUMF1 cDNAs in children with MPSIIIA disease: results of a phase I/II trial. *Hum. Gene Ther* (2014).
19. Barton, D. J., Ludman, M. D., Benkov, K., Grabowski, G. A. & LeLeiko, N. S. Resting energy expenditure in Gaucher's disease type 1: effect of Gaucher's cell burden on energy requirements. *Metabolism* **38**, 1238–1243 (1989).
20. Prasad, K. M. R., Xu, Y., Yang, Z., Acton, S. T. & French, B. A. Robust cardiomyocyte-specific gene expression following systemic injection of AAV: in vivo gene delivery follows a Poisson distribution. *Gene Ther.* **18**, 43–52 (2011).
21. Zeevi, D. A. et al. Proof-of-principle rapid noninvasive prenatal diagnosis of autosomal recessive founder mutations. *J. Clin. Investig.* **125**, 3757–3765 (2015).
22. Verma, J. et al. Inherited metabolic disorders: prenatal diagnosis of lysosomal storage disorders. *Prenat. Diagn.* **35**, 1137–1147 (2015).
23. Pearson, E. G. & Flake, A. W. Stem cell and genetic therapies for the fetus. *Semin. Pediatr. Surg.* **22**, 56–61 (2013).
24. Nivsarkar, M. S. et al. Evidence for contribution of $CD4^+$ $CD25^+$ regulatory T cells in maintaining immune tolerance to human factor IX following perinatal adenovirus vector delivery. *J. Immunol. Res.* **2015**, 397879 (2015).
25. Tai, D. S. et al. Development of operational immunologic tolerance with neonatal gene transfer in nonhuman primates: preliminary studies. *Gene Ther.* (2015).
26. Waddington, S. N. et al. In utero gene transfer of human factor IX to fetal mice can induce postnatal tolerance of the exogenous clotting factor. *Blood* **101**, 1359–1366 (2003).
27. Gray, S. J. et al. Preclinical differences of intravascular AAV9 delivery to neurons and glia: a comparative study of adult mice and nonhuman primates. *Mol. Ther.* **19**, 1058–1069 (2011).
28. U.S. National Institutes of Health, and Recombinant DNA Advisory Committee. Prenatal gene tranfer: scientific, medical, and ethical issues: a report of the Recombinant DNA Advisory Committee. *Hum. Gene Ther.* **11**, 1211–1229 (2000).

Acknowledgements

S.N.W., A.A.R. and J.D.C. received funding from UK Medical Research Council grant G1000709. S.N.W. received funding from MR/N019075/1 and MR/P026494/1 and SPARKS (17UCL01). A.A.R. and S.N.W. received funding from MRC grants MR/R015325/1 and MR/N026101/1 and NC3Rs grant NC/L001780/1. G.M., A.A.R. and S.N.W. received funding from the UK Gauchers Association. A.A.R. received funding from the European Union's Horizon 2020 research and innovation program under grant agreement no. 666918 (BATCure), Action Medical Research (GN2485), MRC grant MR/M00676X/1, Asociación Niemann Pick de Fuenlabrada, Niemann-Pick UK, Niemann Pick Research Foundation and the NBIA Disorders Association. S.M.K.B. and S.N.W. received funding from ERC grant 'Somabio' 260862. C.N.Z.M. received salary support from the Singapore Ministry of Health's National Medical Research Council NMRC/TA/0003/2012 and NMRC/CSA-INV/0012/2016. M.H. is supported by Parkinson's UK grant H-1501. F.M.P. is a Royal Society Wolfson Research Merit Award holder and a Wellcome Trust Investigator in Science. F.M.P. and D.A.P. were supported by the Mizutani Foundation for Glycoscience. J.K.Y.C. is funded by Singapore's Ministry of Health's National Medical Research Council NMRC CSA/043/2012, CSA(SI)/008/2016 and CIRG/1459/2016. J.D.C. received funding from the European Union's Horizon 2020 research and innovation program under grant agreement no. 666918 (BATCure), the Batten Disease Support and Research Association (US) and Batten Disease Family Association (UK). K.M. received funding from the Peto Foundation. S.B. was supported by the National Institute of Health Research (NIHR) UCLH/UCL Biomedical Research Centre. We thank R. Baker, M. Choolani, N. Johana, N. Wen, B. Warburton, S. Richards, T. O'Mahoney, G. Sturges O. Woolmer, E.-H. Davies, T. Collin-Histed, A. Mehta and D. Hughes. Most of all, for guidance, mentorship and inspiration, we thank C. Coutelle.

Author contributions

G.M. contributed murine analysis, immunohistochemistry and manuscript drafting. C.N.Z.M. contributed NHP work and manuscript drafting. A.M.S.W. contributed immunohistochemistry. E.S. contributed mass spectrometry. S.M.K.B. contributed murine analysis. B.R.H. contributed murine analysis. S.K. contributed manuscript drafting. D.P.P. contributed murine analysis. D.B. and S.H. contributed blood spots. A.R.-L. contributed immunohistochemistry. S.B. contributed immunohistochemistry and manuscript drafting. M.H. and D.A.P. contributed immunohistochemistry. F.M.P. contributed immunohistochemistry and manuscript drafting. K.M. contributed mass spectrometry and manuscript drafting. A.B. contributed NHP work. J.D.C. contributed immunohistochemistry and manuscript drafting. J.K.Y.C. contributed NHP work and manuscript drafting. S.H.C. contributed vector generation. S.N.W. contributed murine analysis and manuscript drafting. A.A.R. contributed murine analysis, immunohistochemistry and manuscript drafting.

Competing interests

S.H.C. is an employee at Sanofi, a biopharmaceutical company.

Additional information

Supplementary information is available for this paper at https://doi.org/10.1038/s41591-018-0106-7.

Reprints and permissions information is available at www.nature.com/reprints.

Correspondence and requests for materials should be addressed to S.N.W.

Publisher's note: Springer Nature remains neutral with regard to jurisdictional claims in published maps and institutional affiliations.

Methods

Animal welfare. Mouse procedures and welfare were approved by the University College London Animal Welfare and Ethical Review Board (AWERB) and in accordance with project and personal licenses granted by the UK Home Office and the Animal (Scientific Procedures) Act of 1986. The mouse model for acute neuronopathic Gaucher disease used in this study has been previously described together with all genotyping procedures and primer sequences[2]. Mice heterozygous for mutation in the *Gba* gene and carrying the Cre recombinase gene on a C57BL/6 background were outbred onto WT CD1 mice (Charles River) for five generations. The CD1 strain allows for larger litter size and excellent maternal care of pups. The colony was then maintained using breeding pairs heterozygous for the Gba mutation and carrying the Cre-recombinase gene. Macaque procedures and welfare were approved by and performed in accordance with the Institutional Animal Care and Use Committee (IACUC) at the National University of Singapore and Singapore Health Services Pte., Ltd (IACUC 2009-SHS-512). All in vivo studies performed in macaques were conducted at the SingHealth Experimental Medicine Centre that has been accredited by the Association for Assessment and Accreditation of Laboratory Animal Care International (AAALAC). Potential dams were screened for pre-existing anti-AAV9 antibodies and seronegative females were time-mated. Pregnancies were confirmed, dated and monitored by ultrasound before and after vector delivery.

Histological and immunohistochemical analyses. Experimental cohorts of mice were euthanized by terminal transcardial perfusion using phosphate-buffered saline (PBS), with the exception of P1 mice euthanized by decapitation. Macaque brains and spinal cords were collected following euthanasia using isoflurane and pentobarbitone, cardiac puncture and perfusion of 1% paraformaldehyde.

For free-floating immunohistochemistry-based analyses, the brains were removed and placed into 4% paraformaldehyde solution and stored for 48 h at 4 °C before being cryoprotected in 30% sucrose for a minimum of 24 h at 4 °C. The brains were then serial sectioned along the rostro-caudal axis at 40-µm-thick sections using a freezing microtome (Thermo Fisher Scientific). Immunohistochemical staining was used to detect gene expression. Endogenous peroxidase activity was quenched by incubating sections in 1% H_2O_2 in Tris-buffered saline (TBS) solution for 30 min. Following three washes in TBS, sections were incubated for 30 min in a solution of 15% normal serum in TBS-T (0.3% Triton X-100 in TBS). Subsequently, sections were incubated at 4 °C overnight in primary antibody in TBS-T/10% serum. After rinsing in TBS, the sections were incubated for 2 h in secondary IgG diluted in TBS-T/10% serum. Sections were then rinsed in TBS and incubated for 2 h in a 1:1,000 solution of Vectastain avidin–biotin solution (ABC; Vector Labs). The sections were rinsed in TBS and incubated in 0.05% solution of 3,3′-diaminobenzidine (DAB) containing 0.01% H_2O_2. The staining reaction was stopped by adding ice-cold TBS. The sections were mounted onto chrome-gelatine-coated Superfrost-plus slides (VWR) and left to air-dry overnight. The sections were dehydrated in 70% ethanol, and cleared in xylene for 30 min before being coverslipped using DPX mounting medium. This protocol was used with the following combinations of primary antibodies, blocking serum and secondary antibodies: rat anti-mouse CD68 (1:100; AbD Serotec, MCA1957)[12], rabbit serum and rabbit anti-rat (1:1,000; Vector Laboratories Inc.); mouse anti-GFAP (1:500; Millipore, MAB3402), goat serum and goat anti-mouse (1:1,000; Vector Laboratories Inc.); rabbit anti-LAMP-1 (1:200; Abcam, AB24170), goat serum and goat anti-rabbit (1:1,000; Vector Laboratories Inc.); mouse anti-GBA (N terminus) (1:150; Origene, TA803361), goat serum and goat anti-mouse (1:1,000; Vector Laboratories Inc.); rabbit anti-GBA (C terminus) (1:1,000; Sigma-Aldrich, G4171), goat serum and goat anti-rabbit (1:1,000; Vector Laboratories Inc.); rabbit anti-GFP (1:10,000; Abcam, AB290), goat serum and goat anti-rabbit (1:1,000; Vector Laboratories Inc.), respectively. Brain sections were Nissl-stained using cresyl violet. The sections were incubated in 0.05% cresyl violet in 0.05% acetic acid for 30 min at 60 °C and then washed in deionized water. The sections were differentiated through ascending concentrations of alcohol before being cleared in xylene and coverslipped with DPX.

For histology and immunohistochemical staining on paraffin-embedded tissue sections, mice were euthanized by transcardial perfusion as described above. Brain fixed in 10% buffered formol-saline was embedded in paraffin wax. Microglial activation was examined using an ionized calcium-binding adaptor molecule 1 (Iba1) antibody (Wako Pure Chemical Industries, 019-19741). Immunohistochemistry was performed on automated immunohistochemistry staining machines (Ventana Medical Systems Inc.) using proprietary secondary detection reagents (Ventana Medical Systems Inc.) before development with 3′ 3-diaminobenzedine tetrachloride as the chromogen. Conventional methods were used for Harris hematoxylin and eosin staining. Sections were mounted on chrome-gelatine-coated slides and air-dried overnight. The sections were stained, protected from light, with filtered 0.1% Mayer's hematoxylin (Sigma-Aldrich) for 10 min. The slides were rinsed in distilled water for 5 min and consequently dipped 12 times in 0.5% eosin solution. The sections were quickly washed in distilled water and subsequently dehydrated for 30 s in rising concentrations of ethanol (50%, 70%, 95%, 100%). The slides were finally incubated in Histo-clear for 30 min and coverslipped with DPX mountant medium.

Quantitative analysis of histological and immunohistochemical staining. The quantification of immunohistochemical staining within discrete regions of the brain was conducted by a user blinded to the experimental cohorts. Forty non-overlapping RGB images were taken at ×40 magnification through four consecutive sections within each region of interest. During image capture, all camera and microscope settings were maintained. Regional areas of immunoreactivity were analysed by optical segmentation using Image Pro-Plus (Media Cybernetics). The foreground immunostaining was defined by averaging of the highest and lowest signals and the threshold was set and remained unchanged as each consecutive image was analysed. The data are presented as the mean percentage area of immunoreactivity per field for each discrete region. Stereological counts of neurons by optical fractionation and measurement of cortical thickness and volume were performed using Stereo Investigator (MBF Biosciences)[29]. The grid size and the counting frame used for analysing different brain regions were as follows: S1BF 150 × 150 µm, 50 × 50 µm; VPM/VPL 175 × 175 µm, 50 × 50 µm; Gi 100 × 100 µm, 50 × 50 µm. Cells were counted using a 100× objective. Efficient sampling was estimated by a coefficient of error between 0.05 and 0.1[30]. Four sections for each brain were analysed and the average values of cell counting were used in the calculations.

The mean thickness of the S1BF cortical region was estimated by using the Cavalieri vertical sections principle[31]. The length of ten parallel consecutive lines intersecting perpendicularly the cerebral cortex, traced from the somatosensory barrel cortical layer 1 to the corpus callosum, was measured. Three sections of the midbrain region per each brain were analysed and the average values were reported.

Mass spectrometry. Mouse brains were homogenized in water using an Ultraturax T25 probe homogenizer (IKA). Protein concentrations were determined using bicinchoninic acid (BCA) assay and 200 µg was analyzed for glucosylceramide, glucosylpsychosine and lyso-lactosyl ceramide accumulation. The substrates were extracted in 1 ml of chloroform/methanol (2:1 v/v) containing 80 µg ml^{-1} of d4-C16:0-glucosylceramide internal standard that was synthesized in house[32]. The samples were shaken for 30 min at room temperature before the addition of 200 µl of PBS for phase separation. After a 10 min centrifugation at 16,000*g*, the upper and lower phases were collected and 5 µl of each was injected into the ultraperformance liquid chromatography–tandem mass spectrometry system. Glycosphingolipid reference standards (Matreya) were also analyzed to confirm analyte identity.

The samples were injected onto a Waters ACQUITY UPLC system operated in partial loop mode and separated on a Waters ACQUITY UPLC BEH C18 column (130 Å, 1.7 µm, 2.1 mm × 50 mm) under the following gradient conditions: 0.00–0.20 → 80% A; 0.20–5.00 → 0.1% A; 5.00–9.00 → 0.1% A; 9.01–11.00 → 80% A, where mobile phase A was double-distilled H_2O (ddH_2O) with 0.1% FA; phase B was methanol and the flow rate was 0.65 ml min^{-1}. Column and sample temperatures were kept at 40 °C and 10 °C, respectively. Weak wash solvent was ddH_2O [0.1% FA] and strong wash solvent was acetonitrile/methanol/isopropanol/ddH_2O (1:1:1:1 v/v). The eluting analytes were detected on a Waters XEVO TQ-S triple quadrupole mass spectrometer that was equipped with the electrospray ion source and operated in multiple reaction monitoring and positive ion mode (see Supplementary Table 4 for multiple reaction monitoring details) with the tune page parameters set to achieve the maximum sensitivity for glycosphingolipids as described previously[33]. The data were processed with MassLynx v4.1.

Glycosphingolipid analysis. Glycosphingolipids (GSLs) from brain homogenates were extracted with chloroform/methanol (1:2, v/v) overnight at 4 °C and further purified using solid-phase C18 columns (Telos, Kinesis). GSLs were dried down under nitrogen and treated with either Cerezyme (Genzyme) to obtain glucose from GlcCer, or ceramide glycanase (prepared in house from the medicinal leech *Hirudo medicinalis/verbena*) to obtain oligosaccharides from other GSLs. Liberated glucose and free glycans were then fluorescently labeled with anthranillic acid (2AA). Excess 2AA label was removed using DPA-6S SPE columns (Supelco). Purified 2AA-labeled glucose and 2AA-labeled glycans were separated and quantified by normal-phase high-performance liquid chromatography[34]. The normal-phase high-performance liquid chromatography system consisted of a Waters Alliance 2695 separations module and an in-line Waters 2475 multi λ-fluorescence detector set at excitation $\lambda_{360\,nm}$ and emission $\lambda_{425\,nm}$. The solid phase used was a 4.6 × 250 mm TSK gel-Amide 80 column (Anachem). Results were normalized to protein content determined using BCA assay.

Self-complementary AAV vectors. The human *GBA* cDNA was generated by polymerase chain reaction, verified by DNA sequencing and cloned into the Topo plasmid vector (Invitrogen). A 1.6-kb fragment (containing the open reading frame of the human *GBA* cDNA and bovine growth hormone polyadenylation signal sequence) was then generated by digesting the plasmid with the restriction enzymes NcoI and SpeI and subcloned into a shuttle plasmid containing the scAAV2 inverted terminal repeats and the 0.4 kb GUSB promoter[35] (Supplementary Fig. 8). Recombinant AAV9 serotype vectors encoding *GBA* (scAAV9-GUSB-*GBA*) were generated by the standard triple plasmid transfection method as described previously[36]. Briefly, cell lysates of transfected 293 cells were clarified by centrifugation and then purified by subjecting the preparations to two cycles

of density gradient ultracentrifugation using cesium chloride. The purified recombinant vectors were resuspended and stored in 10 mM sodium phosphate buffer, pH 7.3, containing 180 mM sodium chloride and 0.001% pluronic F68.

AAV administration to mice and macaques. For marker gene studies, we injected CD1 outbred mice. nGD mice were backcrossed onto the CD1 background, to maximize litter sizes and minimize the risk of cannibalization.

We have previously described the administration of gene delivery vectors to the brains of fetal mice[37] and intracerebroventricular injections to neonates has been described in an earlier study[38]. We have previously described intravenous administration to neonatal mice[12]. Briefly, pregnant mice carrying pups at 16 days of gestation were anesthetized using isoflurane inhalation anesthesia and a midline laparotomy was performed to expose the uterus. Five microliters of AAV vector (5×10^{10} genome copies) was administered to all fetuses per dam via a transuterine injection targeting the anterior horn of the lateral ventricle of the left hemisphere of the brain. The laparotomy was sutured and mice were provided topical and systemic analgesia and allowed to recover in a warm chamber. The same dose was administered via intracerebroventricular injection to P0 neonates. The intracerebroventricular injections were directed to the anterior horn of the lateral ventricle. The injection site was identified at 2/5 of the distance from the lambda suture to each eye. P0–P1 mice were anesthetized on ice for 30–60 s. A 33-gauge needle (Hamilton) was inserted perpendicularly at the injection site to a depth of 3 mm and 5 µl of vector was slowly administered. The pup was allowed to recover and placed back into the cage. Forty microliters of AAV vector (4×10^{11} genome copies) was administered to P0 neonates by injection of the superficial temporal vein. At P0–P1, pups were anesthetized on ice for 30–60 s and intravenous injections were performed via the superficial temporal vein using a 33-gauge needle (Hamilton). Once the needle was slowly removed, gentle pressure was applied to the injection site. When the pup fully recovered, it was returned to the dam.

Cynomolgus macaques (*Macaca fasicularis*) were used for non-human primate studies. Macaques underwent time-mating and pregnancy was confirmed through ultrasound evidence of fetal pole and fetal heart activity. Dating of pregnancy was performed as previously reported[39], and IUGT was performed at 0.4G. After induction of anesthesia via sevoflurane, a 25-G Quincke needle (Becton-Dickenson) was used to target the lateral ventricle closest to the anterior maternal abdomen under continuous ultrasound imaging. Vector was injected as a slow bolus (200–350 µl to deliver a total dose of 1.3×10^{12} vg and 2.3×10^{12} vg in each fetus respectively) with ventricular swelling observed as evidence of correct delivery. The needle was removed immediately and the fetus monitored for a further 15 min. A male fetus was delivered naturally and a female fetus was delivered by cesarean section and hand-reared as previously reported. Euthanasia and organ collection were performed on days 0 and 6 respectively under ketamine and isoflurane, via cardiac puncture and exsanguination as previously described[40].

Mouse behavioral studies. Mice underwent foot-fault testing (adapted from ref. [41]) and Rotarod testing (adapted from ref. [42]) at P35, P73 and P100. The operator was blinded to the genotype of the animals throughout the testing period. Briefly, foot-fault testing involved placing a mouse on a stainless-steel grid (41 × 25 cm) with a mesh size of 1 × 1 cm, elevated 30 cm above the bench surface. The number of times a limb fell through the grid (a foot-fault) within 30 s was recorded. Rotarod testing employed a commercially available Rotarod (Harvard Apparatus). Mice were placed on the rotating drum under continuous acceleration (from 4–40 r.p.m. over 5 min), with the latency to fall from the rod, and the speed at which this occurred, measured. Any passive rotations were also noted.

Stereoscopic fluorescence microscopy. GFP expression in various organs was visualized with a stereoscopic fluorescence microscope (MZ16F; Leica). Representative images were captured with a digital microscope camera (DFC420 Leica) and image analysis software (LAS 4.2; Leica). As a result of the differences in the sizes of the organs, intensity of signal and distribution of cells of interest, the images captured were optimized for exposure length and brightness in each case.

GCase enzyme assay. GCase activity was determined using the established synthetic substrate, 4-methylumbelliferone-β-glucopyranoside protocol as previously described[43]. Frozen tissue samples were homogenized with distilled water on ice and the total protein concentration was measured using BCA assay. Samples were incubated with the substrate for 2 h at 37 °C. The reaction was stopped with 1 M glycine buffer, pH 10.4. Fluorescence of the standard 1 nM 4-methylumbelliferone and the samples was read (FluoStar Optima Plate Reader; excitation wavelength: 360 nm, emission wavelength: 450 nm). The enzymatic activity (nmol h^{-1} μg^{-1}) was calculated.

Sample sizes, statistics and randomization. Since the genotypes of injected mice could not be ascertained until after birth, the initial sample size was determined by the number of knockout pups in the uteri of three randomly selected pregnant dams. For most analyses, one-way or two-way ANOVA was performed with either Bonferroni's or Tukey's multiple comparison. The *F* statistic of ANOVA is tolerant of violations in normality, for which we did not test. Nevertheless, mass spectrometry data, which were clearly not normally distributed, were converted by log transformation before ANOVA. Each experiment was performed only once. Behavioral and semi-quantitative scoring were blinded to the investigator.

Reporting Summary. Further information on experimental design is available in the Nature Research Reporting Summary linked to this article.

Data availability. All data generated or analyzed during this study are included in this published article (and its Supplementary Information). Raw data are available online at https://doi.org/10.5281/zenodo.1246085. These data are also available from the corresponding author upon reasonable request.

References

29. Pressey, S. N., Smith, D. A., Wong, A. M., Platt, F. M. & Cooper, J. D. Early glial activation, synaptic changes and axonal pathology in the thalamocortical system of Niemann-Pick type C1 mice. *Neurobiol. Dis.* **45**, 1086–1100 (2012).
30. Gundersen, H. J., Jensen, E. B., Kieu, K. & Nielsen, J. The efficiency of systematic sampling in stereology—reconsidered. *J. Microsc.* **193**, 199–211 (1999).
31. Baddeley, A. J., Gundersen, H. J. & Cruz-Orive, L. M. Estimation of surface area from vertical sections. *J. Microsc.* **142**, 259–276 (1986).
32. Mills, K., Eaton, S., Ledger, V., Young, E. & Winchester, B. The synthesis of internal standards for the quantitative determination of sphingolipids by tandem mass spectrometry. *Rapid Commun. Mass Spectrometry* **19**, 1739–1748 (2005).
33. Auray-Blais, C. et al. Urinary biomarker investigation in children with Fabry disease using tandem mass spectrometry. *Clin. Chim. Acta* **438**, 195–204 (2015).
34. Neville, D. C. et al. Analysis of fluorescently labeled glycosphingolipid-derived oligosaccharides following ceramide glycanase digestion and anthranilic acid labeling. *Anal. Biochem.* **331**, 275–282 (2004).
35. Passini, M. A. et al. Antisense oligonucleotides delivered to the mouse CNS ameliorate symptoms of severe spinal muscular atrophy. *Sci. Transl. Med.* **3**, 72ra18 (2011).
36. Ayuso, E. et al. High AAV vector purity results in serotype- and tissue-independent enhancement of transduction efficiency. *Gene Ther.* **17**, 503–510 (2010).
37. Rahim, A. A. et al. Efficient gene delivery to the adult and fetal CNS using pseudotyped non-integrating lentiviral vectors. *Gene Ther.* **16**, 509–520 (2009).
38. Kim, J. Y., Grunke, S. D., Levites, Y., Golde, T. E. & Jankowsky, J. L. Intracerebroventricular viral injection of the neonatal mouse brain for persistent and widespread neuronal transduction. *J. Vis. Exp.* (2014).
39. Mattar, C. N. Z. et al. Stable human FIX expression after 0.9G intrauterine gene transfer of self-complementary adeno-associated viral vector 5 and 8 in macaques. *Mol. Ther.* **19**, 1950–1960 (2011).
40. Mattar, C. N., Biswas, A., Choolani, M. & Chan, J. K. Animal models for prenatal gene therapy: the nonhuman primate model. *Methods Mol. Biol.* **891**, 249–271 (2012).
41. Lubics, A. et al. Neurological reflexes and early motor behavior in rats subjected to neonatal hypoxic–ischemic injury. *Behav. Brain Res.* **157**, 157–165 (2005).
42. Carter, R. J., Morton, J. & Dunnett, S. B. Motor coordination and balance in rodents. *Curr. Protoc. Neurosci.* **15**, 8.12.1–8.12.14 (2001).
43. Wenger, D. A., Clark, C., Sattler, M. & Wharton, C. Synthetic substrate β-glucosidase activity in leukocytes: a reproducible method for the identification of patients and carriers of Gaucher's disease. *Clin. Genet.* **13**, 145–153 (1978).

nature research

Corresponding author(s): Simon N. Waddington

Reporting Summary

Nature Research wishes to improve the reproducibility of the work that we publish. This form provides structure for consistency and transparency in reporting. For further information on Nature Research policies, see Authors & Referees and the Editorial Policy Checklist.

Statistical parameters

When statistical analyses are reported, confirm that the following items are present in the relevant location (e.g. figure legend, table legend, main text, or Methods section).

n/a	Confirmed	
☐	☒	The exact sample size (*n*) for each experimental group/condition, given as a discrete number and unit of measurement
☐	☒	An indication of whether measurements were taken from distinct samples or whether the same sample was measured repeatedly
☐	☒	The statistical test(s) used AND whether they are one- or two-sided *Only common tests should be described solely by name; describe more complex techniques in the Methods section.*
☒	☐	A description of all covariates tested
☐	☒	A description of any assumptions or corrections, such as tests of normality and adjustment for multiple comparisons
☐	☒	A full description of the statistics including central tendency (e.g. means) or other basic estimates (e.g. regression coefficient) AND variation (e.g. standard deviation) or associated estimates of uncertainty (e.g. confidence intervals)
☐	☒	For null hypothesis testing, the test statistic (e.g. *F*, *t*, *r*) with confidence intervals, effect sizes, degrees of freedom and *P* value noted *Give P values as exact values whenever suitable.*
☒	☐	For Bayesian analysis, information on the choice of priors and Markov chain Monte Carlo settings
☒	☐	For hierarchical and complex designs, identification of the appropriate level for tests and full reporting of outcomes
☒	☐	Estimates of effect sizes (e.g. Cohen's *d*, Pearson's *r*), indicating how they were calculated
☐	☒	Clearly defined error bars *State explicitly what error bars represent (e.g. SD, SE, CI)*

Our web collection on statistics for biologists may be useful.

Software and code

Policy information about availability of computer code

Data collection	The evaluation of the immunoreactivity of stained sections was performed using the Image-Pro Premier analysis system (Media Cybernetics, Rockville MD, USA). Neuron counting and cortical thickness measurements were estimated with Stereo Investigator software (MBF Bioscience, Williston VE, USA).
Data analysis	The statistical analysis was performed with GraphPad Prism Software (v. 6.0e). The evaluation of the immunoreactivity of stained sections was performed using the Image-Pro Premier analysis system (Media Cybernetics, Rockville MD, USA). Neuron counting and cortical thickness measurements were estimated with Stereo Investigator software (MBF Bioscience, Williston VE, USA).

For manuscripts utilizing custom algorithms or software that are central to the research but not yet described in published literature, software must be made available to editors/reviewers upon request. We strongly encourage code deposition in a community repository (e.g. GitHub). See the Nature Research guidelines for submitting code & software for further information.

Data

Policy information about availability of data

All manuscripts must include a data availability statement. This statement should provide the following information, where applicable:

- Accession codes, unique identifiers, or web links for publicly available datasets
- A list of figures that have associated raw data
- A description of any restrictions on data availability

All data generated or analysed during this study are included in this published article (and its supplementary information files). Raw data are available online at 10.5281/zenodo.1246085. These data are also available from the corresponding author on reasonable request.

Field-specific reporting

Please select the best fit for your research. If you are not sure, read the appropriate sections before making your selection.

☒ Life sciences ☐ Behavioural & social sciences ☐ Ecological, evolutionary & environmental sciences

For a reference copy of the document with all sections, see nature.com/authors/policies/ReportingSummary-flat.pdf

Life sciences study design

All studies must disclose on these points even when the disclosure is negative.

Sample size	The group sizes were determined by a power calculation (power of 0.8), using PS Power & Sample size software (Dupont WD, Plummer WD, Jr. (1990). Power and sample size calculations. A review and computer program. Control Clin Trials 11(2): 116-128.). The calculation was based upon differences between groups obtained in our previous study (Rahim AA et al (2011). Intravenous administration of AAV2/9 to the fetal and neonatal mouse leads to differential targeting of CNS cell types and extensive transduction of the nervous system. FASEB J 25(10): 3505-3518.). We aimed to include two additional mice in each group in case of unexpected loss from the study (which did not occur)
Data exclusions	No data were excluded from the analyses.
Replication	All data using AAV9-GUSB-GBA vector are presented in this manuscript. We have repeated intracranial and intravenous neonatal injections using an alternative vector configuration and observe similar therapeutic efficacy
Randomization	For fetal injections, randomization was inevitable since the genotype of the injected fetuses could not be determined until after birth. Neonatal pups were randomly allocated to separate treated and untreated groups, ensuring random distribution across litters
Blinding	The operator was blinded to the genotype of the animals throughout testing and analysis of behavioral scoring. The quantification of immunohistochemical staining and stereological count of neurons were conducted by a user blinded to the experimental cohorts.

Reporting for specific materials, systems and methods

Materials & experimental systems

n/a	Involved in the study
☒	☐ Unique biological materials
☐	☒ Antibodies
☒	☐ Eukaryotic cell lines
☒	☐ Palaeontology
☐	☒ Animals and other organisms
☒	☐ Human research participants

Methods

n/a	Involved in the study
☒	☐ ChIP-seq
☒	☐ Flow cytometry
☒	☐ MRI-based neuroimaging

Antibodies

Antibodies used	Rabbit anti-GFP, AB290, Abcam; Mouse anti-GBA1 N-terminus, clone OTI1D12, TA803361, Origene; Anti-GBA1 C-terminus, G4171, Sigma-Aldrich.; Rat anti-mouse CD68, MCA1957, AbD Serotech.; Mouse anti-GFAP, MAB3402, Millipore.; Rabbit anti-LAMP1, AB24170, Abcam.; Biotinylated anti-mouse IgG, BA-9200, Vector Lb Inc.; Biotinylated anti-rabbit IgG, BA-1000, Vector Lb Inc.; Biotinylated anti-rat IgG, BA-9400, Vector Lb Inc.; Lot numbers were not recorded

Validation	Rabbit anti-GFP, AB290, Abcam: suitable for IHC-FrFl analysis of mouse brain tissue sections (from abcam.com). Anti-GBA1 raised against amino acids 40-315 of human GBA; Origene: suitable for WB and IHC (from origene.com) Anti-GBA1 C-terminus, G4171, Sigma-Aldrich: mouse reactivity (from abcam.com), suitable for IHC (see data in the manuscript). Rat anti-mouse CD68, MCA1957, AbD Serotech: suitable for immunohistology of mouse tissue sections (from bio-rad-antibodies.com). Mouse anti-GFAP, MAB3402, Millipore: suitable for IHC of mouse tissue (from merckmillipore.com). Rabbit anti-LAMP1, AB24170, Abcam: suitable for IHC of mouse tissue (from abcam.com). Biotinylated secondary antibodies, Vector Lb Inc: suitable for tissue staining (from vectorlabs.com).

Animals and other organisms

Policy information about studies involving animals; ARRIVE guidelines recommended for reporting animal research

Laboratory animals	Mice heterozygous for mutation in the GBA1 gene and carrying the Cre recombinase gene on a C57BL/6 background were outbred onto wild type CD1 mice (Charles River, Harlow, UK) for five generations. Fig 2F-M fetal IV treated KO: 3 females 2 males. Sex not recorded for Fig 2A-E IV treated KO Fig 4A-M neonatal IV treated KO: 4 males, 1 female. WT: 2 males, 1 female. IC treated KO: 1 male, 2 females. Sex not recorded for Fig 4N-P 1 male cynomolgus macaque, in utero injection at D58, Delivery at D147, Euthanasia at day 0. 1 female cynomolgus macaque in utero injection at D59, Caesarean delivery at D147, Euthanasia on day 6
Wild animals	No wild animals were used in this study
Field-collected samples	No field-collected samples were used in this study